J|A|C|S
ARTICLES
Published on Web 02/23/2005

Periodic Hexagonal Mesostructured Chalcogenides Based on Platinum and $[SnSe_4]^{4-}$ and $[SnTe_4]^{4-}$ Precursors. Solvent Dependence of Nanopore and Wall Organization

Pantelis N. Trikalitis,[†,§] Thomas Bakas,[‡] and Mercouri G. Kanatzidis*[,†]

Contribution from the Department of Chemistry, Michigan State University, East Lansing, Michigan, 48824, and Department of Physics, University of Ioannina, Ioannina, 45110 Greece

Received August 30, 2004; E-mail: Kanatzid@cem.msu.edu

Abstract: Mesostructured chalcogenide-based materials with long-range order and semiconducting properties can be prepared using suitable molecular building blocks, linkage metal ions and surfactant molecules. In this paper we present surfactant templated, open framework platinum tin selenide and telluride materials assembled using K_4SnQ_4 (Q = Se, Te) salts and K_2PtCl_4 as precursors and a study of pore and wall organization. We find that materials prepared in water exhibit disordered pore organization, whereas those prepared in formamide are long-range ordered with hexagonal symmetry. In formamide the $[SnQ_4]^{4-}$ anions undergo condensation−oligomerization reactions that produce different chalcogenido molecular species, whereas in water the anions remain intact. In addition to solvent, the pore organization and overall quality of the mesostructured materials strongly depend on the surfactant molecules, i.e., chain length and headgroup size. For example, highly ordered mesostructured platinum tin selenides with hexagonal symmetry were obtained using the hydroxyl-functionalized surfactants $C_nH_{2n+1}N(CH_3)(CH_2CH_2OH)_2Br$ (n = 16, 18, and 20), but when the headgroup was triethylammonium, hexagonal pore order was achieved only for n = 20 and not for n = 16 and 18. The experimental results imply that in order to achieve highly ordered chalcogenide frameworks a single building anionic block might be insufficient. Finally, we also report the first examples of hexagonal mesostructured Pt/Sn/Te materials based on K_4SnTe_4 as the precursor. The tellurides behave differently for their selenium analogues and have very low energy band gaps, in the range 0.5−0.7 eV.

Introduction

Non-oxidic porous materials such as metal chalcogenides represent a special class of solids that could combine porosity and optoelectronic functionality in a single system promising new capabilities. For this reason, research involving open-framework chalcogenide-based materials with both microporous and mesoporous structures is attracting considerable attention.[1−5] Although mesoporous chalcogenides are still scarce,[6] mesostructured materials with occupied pores are now possible and of equal importance because they can give rise to interesting properties.[7,8] Our group and others succeeded in synthesizing surfactant-templated semiconducting mesostructured materials based on discrete chalcogenido building blocks $[SnSe_4]^{4-}$, $[Sn_2S_6]^{4-}$, $[Sn_2Se_6]^{4-}$, $[Ge_4S_{10}]^{4-}$, $[Ge_4Se_{10}]^{4-}$, and $[Sn_4Se_{10}]^{4-}$ and various linkage metal ions (Mn^{2+}, Fe^{2+}, Co^{2+}, Ni^{2+}, Zn^{2+}, Cd^{2+}, Hg^{2+}, Ga^{3+}, In^{3+}, Sb^{3+}, Sn^{4+}, Pt^{2+}, Pd^{2+}).[9,10] These non-oxidic systems form predominantly through a controlled electrostatic assembly mechanism. We know that the nature of the chalcogenide anions, the linkage metal, and the surfactant molecules are important factors that determine the final product in terms of pore order, pore symmetry, thermal stability, and overall structural quality. For example, in the case of adamantane

[†] Michigan State University.
[‡] University of Ioannina.
[§] Current address: Department of Chemistry, University of Crete, Heraklion, Greece.

(1) (a) Li, H. L.; Laine, A.; O'Keeffe, M.; Yaghi, O. M. *Science* **1999**, *283*, 1145−1147. (b) Li, H. L.; Kim, J.; O'Keeffe, M.; Yaghi, O. M. *Angew. Chem., Int. Ed.* **2003**, 42, 1819−1821 (c) Bedard, R. L.; Wilson, S. T.; Vail, L. D.; Bennett, J. M.; Flanigen, E. M. In *Zeolites: Facts, Figures, Future. Proceedings of the 8th International Zeolite Conference*; Jacobs, P. A.; van Santen, R. A., Eds.; Elsevier: Amsterdam, 1989; pp 375−387. (d) Yaghi, O. M.; Sun, Z.; Richardson, D. A.; Groy, T. L. *J. Am. Chem. Soc.* **1994**, *116*, 807−808. (e) Bowes, C. L.; Ozin, G. A. *Adv. Mater.* **1996**, *8*, 13. (f) Cahill, C. L.; Parise, J. B. *J. Chem. Soc., Dalton Trans.* **2000**, *9*, 1475−1482.
(2) (a) MacLachlan, M. J.; Coombs, N.; Ozin, G. A. *Nature* **1999**, *397* (6721), 681−684. (b) Trikalitis, P. N.; Bakas, T.; Papaefthymiou, V.; Kanatzidis, M. G. *Angew. Chem., Int. Ed.* **2000**, *39* (24), 4558−4562.
(3) Su, W. P.; Huang, X. Y.; Li, J.; Fu, H. X. *J. Am. Chem. Soc.* **2002**, *124* (44), 12944−12945. (b) Cahill, C. L.; Ko, Y. H.; Parise, J. B. *Chem. Mater.* **1998**, *10*, 19−21.
(4) (a) Zheng, N. F.; Bu, X. G.; Wang, B.; Feng, P. Y. *Science* **2002**, *298*, 2366−2369. (b) Bu, X. H.; Zheng, N. F.; Wang, X. Q.; Wang, B.; Feng, P. Y. *Angew. Chem., Int. Ed.* **2004**, *43* (12), 1502−1505 (c) Wang, C.; Bu, X. H.; Zheng, N. F.; Feng, P. Y. *Angew. Chem., Int. Ed.* **2002**, *41*, 1959. (d) Zheng, N. F.; Bu, X. H.; Feng, P. Y. *Nature* **2003**, 426 (6965), 428−432.
(5) Riley, E.; Tolbert, S. H. *J. Am. Chem. Soc.* **2003**, *125*, 4551
(6) (a) Vanchura, B. A.; He, P. G.; Antochshuk, V.; Jaroniec, M.; Ferryman, A.; Barbash, D.; Fulghum, J. E.; Huang, S. D. *J. Am. Chem. Soc.* **2002**, *124* (41), 12090−12091. (b) Li, J. Q.; Kessler, H.; Soulard, M.; Khouchaf, L.; Tuilier, M. H. *Adv. Mater.* **1998**, *10*, 946.
(7) Mesostructured materials are those possessing pores featured in the mesoscale regime (2−50 nm). Mesoporous materials are a subclass of mesostructured ones and possess accessible pores.
(8) Wang, J.; Stucky, G. D. *Adv. Funct. Mater.* **2004**, *14*, 409−415 and references therein.

10.1021/ja0447614 CCC: $30.25

clusters $[Ge_4Q_{10}]^{4-}$ (Q = S, Se) and $[Sn_4Se_{10}]^{4-}$ the use of Pt^{2+} as the linking metal and pyridinium-based surfactant leads to materials with exceptionally high hexagonal pore order.[9c] When the smaller $[Sn_2Se_6]^{4-}$ anions and Pt^{2+} ion are used materials with cubic $Ia\bar{3}d$ symmetry and single-crystal particle morphology are obtained.[11] These systems have accessible pores via ion-exchange processes.

In this work we describe mesostructured materials from $[SnSe_4]^{4-}/Pt^{2+}$ and $[SnTe_4]^{4-}/Pt^{2+}$ combinations featuring hexagonal MCM-41 type symmetry. Although disordered mesostructured metal tin tellurides have been described,[5] we have succeeded in producing a new variety with ordered hexagonal pores. Materials prepared in water exhibit disordered structures, whereas those prepared in formamide (FM) possess good hexagonal order. To explain this we performed solution ^{119}Sn NMR spectroscopy of the precursor anions and found that in FM (but not in water) both $[SnSe_4]^{4-}$ and $[SnTe_4]^{4-}$ undergo conversions to $[Sn_2Q_6]^{4-}$ and Q^{2-} and these species get incorporated into the ensuing structure. The results reported here lead to the proposition that in order to form mesostructures with long-range order, more than one chalcogenido fragment may be desirable.

Experimental Section

Starting Materials. K_4SnSe_4 was prepared according to published procedure.[12] K_4SnTe_4 was prepared in high yield and pure form by a method developed in our laboratory. K_2PtCl_4 was purchased from Strem Chemical Inc. Cetylpyridinium bromide monohydrate ($C_{16}PyBr\cdot H_2O$), cetyltrimethylammonium bromide ($C_{16}N(CH_3)_3Br$), and formamide (FM) were purchased from Aldrich. The other surfactants $C_nH_{2n+1}N(C_5H_5)Br$ (denoted as C_nPyBr, n = 12, 14, and 18), $C_nH_{2n+1}N(CH_3)_3Br$ (n = 18 and 20), $C_nH_{2n+1}N(CH_2CH_3)Br$ (n = 16, 18, and 20), and $C_nH_{2n+1}N(CH_3)(CH_2CH_2OH)_2Br$ (n = 16, 18, and 20) were synthesized by refluxing the corresponding alkyl-bromide with an excess of pyridine, trimethylamine, triethylamine, and methyl-diethanolamine, respectively, in ethanol. The solvent was removed using a rotary evaporator, and pure compounds were obtained in high yield (>90%) after a single recrystallization from $CHCl_3$−ethyl acetate.

Mesostructured Platinum Tin Selenides. All reactions were carried out inside a glovebox under nitrogen. In a typical preparation 0.591 g (1.00 mmol) of K_4SnSe_4 was dissolved in 20 mL of FM at 80 °C forming a clear red-orange solution. To this solution, 4 g of surfactant were added, and after a few minutes a clear deep-red solution was formed. In a separate flask 0.415 g (1 mmol) of K_2PtCl_4 in 10 mL of FM was heated at 80 °C to form a red-orange solution, and this was added to the surfactant/K_4SnSe_4 solution over a period of 2 min using a pipet. A dark brown-red solid was formed within a few seconds, and the mixture was stirred overnight at 80 °C. The product was isolated by filtration, washed with copious amount of warm (80 °C) FM and H_2O, and dried under vacuum. Yield: >80% based on K_4SnSe_4. The same materials alternatively can be synthesized by first mixing the K_4SnSe_4/FM and K_2PtCl_4/FM solutions and subsequently adding the mixture dropwise into the surfactant/FM solution at 80 °C.

Mesostructured Platinum Tin Tellurides. All reactions were carried out inside a glovebox under nitrogen. In a typical preparation 4 g of surfactant were dissolved in 20 mL of FM at 80 °C. In separate flasks 0.785 g (1.00 mmol) of K_4SnTe_4 and 0.415 g (1 mmol) of K_2PtCl_4 dissolved in 10 mL of FM at 80 °C forming deep-red and red-orange solutions, respectively. These solutions were added simultaneously to the surfactant solution. A black solid formed immediately, and the mixture was aged overnight at 80 °C under stirring. The product was isolated by filtration, washed with copious amount of warm (80 °C) FM and H_2O, and dried under vacuum. Yield: >80% based on K_4SnTe_4.

For convenience we represent these materials as *surf*-Pt_SnQ_4,[13] where *surf* = surfactant molecule and Pt and SnQ_4 are the metal and chalcogenide anion used as the precursors.

Physical Measurements. Characterization procedures and methods involving X-ray diffraction, thermogravimetric analyses (TGA), C, H, and N elemental analysis, UV/vis/near-IR spectroscopy, Mössbauer spectroscopy, scanning and transmission electron microscopy, and energy dispersive analysis have been described in detail elsewhere.[9] Solution ^{119}Sn NMR spectra were obtained at room temperature without locking on Varian VXS-300S (7.05 T). The spectrometer frequency was 111.8187 MHz for ^{119}Sn. Relaxation delays were not applied. The pulse width setting was 7.75 μs. Line-broadening parameters used in the exponential multiplication of the free-induction decays were 30−50 Hz. Samples for NMR spectroscopy were prepared by dissolving 0.5 mmol of K_4SnQ_4 in 10 mL of solvent (FM or H_2O) at room temperature. The same concentration was used for the synthesis of the mesostructured materials. Solutions that were heated at 80 °C prior to the measurement show the same ^{119}Sn NMR spectra as compared to those prepared at room temperature.

Results and Discussion

We describe herein a new family of platinum-based mesostructured materials with semiconducting properties by employing $[SnSe_4]^{4-}$ as the precursor. In doing so, we have used a set of surfactants with varying chain length and headgroup size in order to probe their effect on the quality of the mesostructure. We also examined for the first time the effect of solvent in this chemistry, namely FM versus water. The effects are profound with FM producing mesostructured materials with well ordered pores, whereas H_2O gives products with disordered pores.

Furthermore, we extended the scope of these systems by employing $[SnTe_4]^{4-}$ to generate the tellurium analogues. The properties of the mesostructured Pt/Sn/Te systems are significantly different from those of the selenides. The Pt/Sn/Te systems exhibit significantly higher pore order than a related set of mesostructured platinum tin tellurides reported recently.[5]

Despite the simplicity of the $[SnSe_4]^{4-}$ anion, the chemistry associated with the formation of mesostructured frameworks is rather complex. Many questions remain outstanding. For example, does the precursor molecule remain intact in the product? If yes, is it the only species present or are there other selenide species as well? If not, what is its fate? Does the elemental composition of the product change with surfactant or surfactant length? Why does one obtain products of very different pore order and quality from water vis-à-vis FM?

One way to approach these issues is to examine the precursor solutions before adding the linking metal to initiate the assembly

(9) (a) Rangan, K. K.; Billinge, S. J. L.; Petkov, V.; Heising, J.; Kanatzidis, M. G. *Chem. Mater.* **1999**, *11*, 2629−2632. (b) Wachhold, M.; Rangan, K. K.; Lei, M.; Thorpe, M. F.; Billinge, S. J. L.; Petkov, V.; Heising, J.; Kanatzidis, M. G. *J. Solid State Chem.* **2000**, *152*, 21−36. (c) Trikalitis, P. N.; Rangan, K. K.; Kanatzidis, M. G. *J. Am. Chem. Soc.* **2002**, *124*, 2604−2613. (d) Rangan, K. K.; Trikalitis, P. N.; Canlas, C.; Bakas, T.; Weliky, D. P.; Kanatzidis, M. G. *Nano Lett.* **2002**, *2*, 513−517. (e) Trikalitis, P. N.; Rangan, K. K.; Bakas, T.; Kanatzidis, M. G. *Nature* **2001**, *410*, 671−675. (f) Rangan, K. K.; Trikalitis, P. N.; Bakas, T.; Kanatzidis, M. G. *Chem. Commun.* **2001**, 809−810. (g) Rangan, K. K.; Trikalitis, P. N.; Kanatzidis, M. G. *J. Am. Chem. Soc.* **2000**, *122*, 10230−10231.

(10) MacLachlan, M. J.; Coombs, N.; Bedard, R. L.; White, S.; Thompson, L. K.; Ozin, G. A. *J. Am. Chem. Soc.* **1999**, *121*, 12005−12017.

(11) Trikalitis, P. N.; Rangan, K. K.; Bakas, T.; Kanatzidis, M. G. *J. Am. Chem. Soc.* **2002**, *124*, 12255−12260.

(12) Klepp, K. O. *Z. Naturforsch., B: Chem. Sci.* **1992**, *47*, 411−417.

(13) The notation *surf*-Pt_SnQ_4 is meant to indicate a material based on surfactant, Pt^{2+} and having derived from a $[SnQ_4]^{4-}$ precursor. It is not meant to indicate a specific stoichiometry or formula or to indicate that the materials contain the $[SnQ_4]^{4-}$ anion in the structure.

reaction. Namely, ^{119}Sn NMR spectroscopy can provide some clues as to what happens to $[SnSe_4]^{4-}$ and $[SnTe_4]^{4-}$ in FM and water under conditions that are similar to those during synthesis. Indeed these experiments show clear signs of the intricate chemistry of these anions in FM, along with implications for the nature of the resulting products.

Behavior of $[SnQ_4]^{4-}$ (Q = Se, Te) Precursors in Solution. The K_4SnQ_4 (Q = Se, Te) salts are highly soluble in water and FM giving solutions that persist for weeks. The anions however are labile, and equilibria are quickly established creating new species. The chemistry strongly depends on solvent and the presence of other chemical species (e.g., Lewis acids). FM is the solvent employed for the synthesis of mesostructured chalcogenides; therefore, it is important to identify the anions present in it, since each one is a potential building block to the structure of the final product.

A powerful method for the identification and characterization of metal chalcogenide anions in solution is multinuclear NMR spectroscopy. In the past, several seleno- and tellurostannate anions in NH_3 and ethylenediamine have been studied by ^{119}Sn, ^{77}Se, and ^{125}Te NMR spectroscopy including the $[SnQ_4]^{4-}$, $[Sn_2Q_6]^{4-}$, $[Sn_2Q_7]^{4-}$, and $[Sn_4Se_{10}]^{4-}$ (Q = Se, Te). [14,15] Because the ^{119}Sn NMR signals of all these are markedly different, the technique is an excellent tool for identifying these anions in solution.

The ^{119}Sn NMR spectrum of K_4SnSe_4 in H_2O consists of a singlet at −420.6 ppm flanked by one pair of ^{77}Se satellites with ^{119}Sn−^{77}Se coupling constant 1491 Hz and a trace impurity signal at −473.4 ppm, Figure 1a. This signal is the fingerprint of the $[SnSe_4]^{4-}$ anion[14] and indicates its integrity in water.

The ^{119}Sn NMR spectrum of K_4SnSe_4 dissolved in FM shows two different signals, Figure 1b. The signal located at −454.8 ppm, and its pair of ^{77}Se satellites (^{119}Sn−^{77}Se coupling constant 1515 Hz) corresponds to the $[SnSe_4]^{4-}$ anion. The signal centered at −481.2 ppm shows two pairs of ^{77}Se satellites with ^{119}Sn−^{77}Se coupling constants 1917 and 918 Hz, respectively, and correspond to the $[Sn_2Se_6]^{4-}$ anion.[14] Clearly in FM the $[SnSe_4]^{4-}$ anions undergo condensation to dimeric $[Sn_2Se_6]^{4-}$ presumably releasing Se^{2-} ions in solution.[16] The degree of condensation in FM was found to be time dependent. Freshly prepared samples contained both types of anions; however, after hours, the equilibrium shifted toward $[Sn_2Se_6]^{4-}$ and 2 day old samples showed only $[Sn_2Se_6]^{4-}$. The reason for the different behaviors in the two solvents is not clear given the similarities of these solvents in terms of dielectric constant and extent of

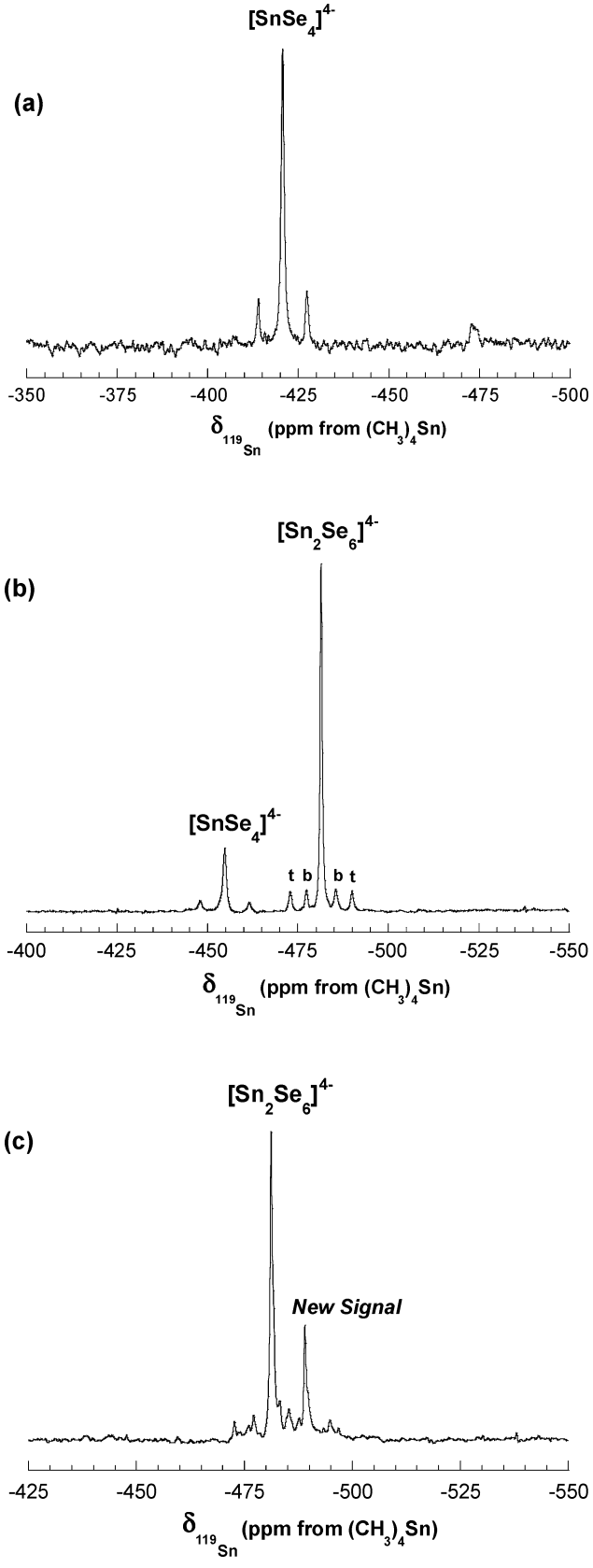

Figure 1. ^{119}Sn NMR spectrum of K_4SnSe_4 dissolved in (a) H_2O, (b) FM, and (c) the presence of K_2PtCl_4 in FM. The symbols t and b denote satellite doublets arising from ^{119}Sn−^{77}Se coupling of terminal and bridging selenide atoms, respectively. Corresponding ^{119}Sn NMR experiments of solutions containing K_4SnQ_4 and surfactant indicated the same $[Sn_xSe_y]^{2-}$ anions as in the surfactant-free solutions.

(14) (a) Campbell, J.; Devereux, L. A.; Gerken, M.; Mercier, H. P. A.; Pirani, A. M.; Schrobilgen, G. J. *Inorg. Chem.* **1996**, *35*, 2945−2962. (b) Campbell, J.; Diciommo, D. P.; Mercier, H. P. A.; Pirani, A. M.; Schrobilgen, G. J.; Willuhn, M. *Inorg. Chem.* **1995**, *34*, 6265−6272. (c) Burns, R. C.; Devereux, L. A.; Granger, P.; Schrobilgen, G. J. *Inorg. Chem.* **1985**, *24*, 2615−2624.

(15) Krebs investigated the aqueous solution behavior of some monomeric thio- and selenogermanates and stannates anions $[MQ_4]^{4-}$, (M = Ge, Sn; Q = S, Se) and showed the existence of other polynuclear species $[M_2Q_6]^{4-}$ and $[M_4Q_{10}]^{4-}$ as products from condensation reactions. The presence of these polynuclear anions in aqueous solution is highly dependent on the pH and in some cases there is a significant overlap in the pH ranges of existence. Presumably in the overlapping pH regions the species are in equilibrium. Corresponding studies in nonaqueous solvents are scarce. Krebs, B. *Angew. Chem., Int. Ed. Engl.* **1983**, *22*, 113−134.

(16) This reaction may be facilitated by the presence of adventitious protons in FM (e.g., from H_2O, formic acid, etc.). Therefore the Se^{2-} ions could exist as $[SeH]^-$. The same behavior was observed in Na_4SnS_4 where ^{119}Sn NMR experiments showed the $[SnS_4]^{4-}$ anions are intact in water while in FM they convert to $[Sn_2S_6]^{4-}$.[9d]

hydrogen bonding. It is possible that adventitious protons (derived from decomposition of FM molecules) might be responsible.

The effect of adding K_2PtCl_4 on the condensation of $[SnSe_4]^{4-}$ in H_2O and FM was also investigated. The ^{119}Sn NMR spectrum of K_4SnSe_4 and K_2PtCl_4 dissolved in FM in a 2:1 ratio shows the presence of $[Sn_2Se_6]^{4-}$ and another signal centered at −489 ppm which could not be assigned to any known selenostannate anion, Figure 1c.[17]

The solution behavior of $[SnTe_4]^{4-}$ is very similar to $[SnSe_4]^{4-}$. Figure 2a shows the ^{119}Sn NMR spectrum of K_4SnTe_4 in H_2O that consists only of one signal centered at −1659 ppm flanked by a pair of ^{125}Te satellites with $^{119}Sn-^{125}Te$ coupling constant 3015 Hz, characteristic of the intact $[SnTe_4]^{4-}$ anion.[14] The corresponding ^{119}Sn NMR spectrum in FM shows two different signals, Figure 2b. One is centered at −1675 ppm followed by two pairs of ^{125}Te satellites with $^{119}Sn-^{125}Te$ coupling constants 3783 and 1670 Hz, respectively, and corresponds to the $[Sn_2Te_6]^{4-}$ anion.[14] A second signal at −1718 ppm followed by a pair of ^{125}Te satellites with a coupling constant of 3076 Hz is due to $[SnTe_4]^{4-}$. Figure 2c shows the ^{119}Sn NMR spectrum of a mixture of K_4SnTe_4 and K_2PtCl_4 dissolved in FM in a 2:1 ratio, which shows four different signals. Those centered at −1675 and −1722 ppm are characteristic of $[Sn_2Te_6]^{4-}$ and $[SnTe_4]^{4-}$, respectively. The peaks at −1630 and −1638 ppm are new and could not be assigned to known tellurostannate anions and may be due to $Pt^{2+}/[Sn_2Te_6]^{4-}$ complexes.

To observe how acidity affected the distribution of the $[Sn_xSe_y]^{n-}$ anions, we added protons (acetic acid) in $[SnSe_4]^{4-}$ solutions (water and FM).[18] Indeed protons greatly shifted the equilibria taking place in H_2O upon controlled acidification (∼1 equiv), while in FM only $[Sn_2Se_6]^{4-}$ was detected;[19] however, adding excess acetic acid in FM resulted in the appearance of $[Sn_4Se_{10}]^{4-}$ anions as well. Since linking metal ions such as Pt^{2+} are themselves Lewis acids we can expect their presence to play a role in the condensation−oligomerization reactions of $[SnSe_4]^{4-}$ anions during framework assembly.

These results provide certain insights regarding mesostructured metal chalcogenide materials produced in FM. First, the linking metals could be influencing dynamically the distribution of anionic species such as $[SnSe_4]^{4-}$, $[Sn_2Se_6]^{4-}$, and Se^{2-}. Their relative ratio would be determined by the Lewis acidity and concentration of the metal, its coordination preference, and temperature. Second, we can infer that in FM the singular inclusion of the precursor $[SnSe_4]^{4-}$ ions in the structure is unlikely. Probably $[Sn_2Se_6]^{4-}$ and Se^{2-} or a combination of all three $[SnSe_4]^{4-}/[Sn_2Se_6]^{4-}/Se^{2-}$ (perhaps even some $[Sn_4Se_{10}]^{4-}$) are incorporated in the framework, each playing a role in building and stabilizing the overall structure.

Synthesis of the Mesophases and the Nature of the Inorganic Framework. A summary of the analytical and other data for the mesostructured materials reported here is given in Table 1. The ratio of Pt/Sn was found in all cases to be very close to the value expected from the synthesis (1:1). The Q/Sn ratio varied slightly among the different members but averaged around 4:1. In a few cases however we observed Se deficiency (e.g., Q/Sn ratio 3.6:1; see Table 1). As we present below the mesostructured pore organization and overall quality strongly depend on the nature of the surfactant. These parameters

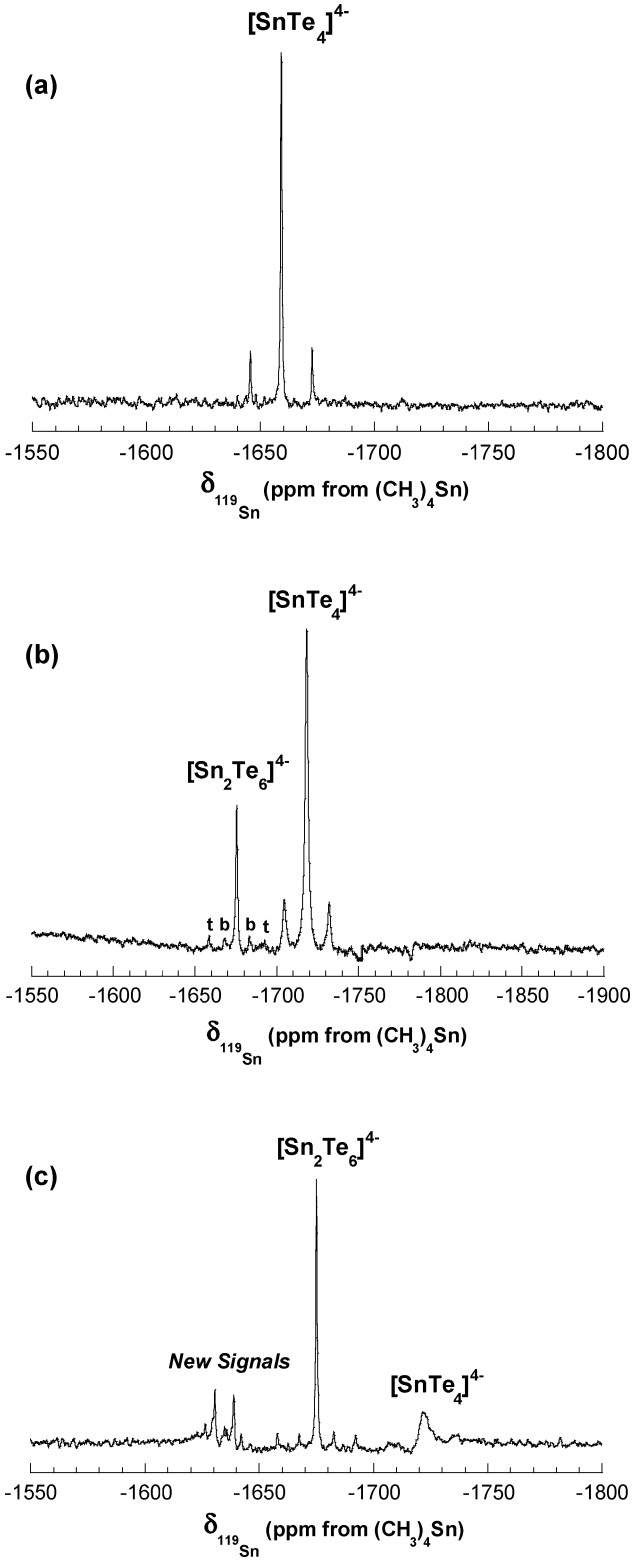

Figure 2. ^{119}Sn NMR spectrum of K_4SnTe_4 dissolved in (a) H_2O, (b) FM, and (c) the presence of K_2PtCl_4 in FM. The symbols t and b denote satellite doublets arising from $^{119}Sn-^{125}Te$ coupling of terminal and bridging telluride atoms, respectively.

(17) A similar spectrum was recorded in water. This new signal could be due to a higher $[Sn_xSe_y]^{z-}$ oligomer or due to a soluble Pt/Sn/Se complex.
(18) The introduction of Lewis acid centers, such as linkage metal ions to $[SnSe_4]^{4-}$ solutions, increases the overall acidity of the solution.
(19) Based on ^{119}Sn NMR spectra of solutions containing K_4SnSe_4 and CH_3COOH in stoichiometric 1:1 molar ratio.

Table 1. Summary of Elemental Analyses, Colors, and Energy Band Gaps for the Mesostructured Platinum Tin Chalcogenides

mesophase[13]	% C, H, N	TGA wt loss, %	Pt/Sn/Q[a]	color	band gap, eV
$C_{12}PyPt\_SnSe_4$	26.36, 4.01, 2.03	27.9	1.0:1:3.7	dark brown-red	1.45
$C_{14}PyPt\_SnSe_4$	33.40, 5.27, 2.25	35.4	1.1:1:3.8	dark brown-red	1.57
$C_{16}PyPt\_SnSe_4$	32.11, 5.01, 1.73	37.8	1.2:1:3.7	dark brown-red	1.65
$C_{18}PyPt\_SnSe_4$	38.90, 6.24, 2.22	39.9	1.2:1:3.9	dark brown-red	1.57
$C_{16}N(CH_3)_3Pt\_SnSe_4$	25.82, 4.78, 1.80	33.5	1.2:1:4.3	dark brown-red	1.38
$C_{18}N(CH_3)_3Pt\_SnSe_4$	29.40, 5.45, 1.77	36.1	1.1:1:3.7	dark brown-red	1.58
$C_{20}N(CH_3)_3Pt\_SnSe_4$	33.04, 6.18, 1.83	41.0	1.1:1:3.8	dark brown-red	1.64
$C_{16}N(CH_2CH_3)_3Pt\_SnSe_4$	31.01, 5.75, 1.31	38.7	1.1:1:3.9	dark brown-red	1.57
$C_{18}N(CH_2CH_3)_3Pt\_SnSe_4$	30.56, 5.78, 1.45	38.5	1.1:1:3.6	dark brown-red	1.63
$C_{20}N(CH_2CH_3)_3Pt\_SnSe_4$	32.55, 6.10, 2.01	43.5	1.0:1:3.6	dark brown-red	1.43
$C_{16}N(CH_3)(CH_2CH_2OH)_2Pt\_SnSe_4$	34.24, 6.57, 1.99	46.8	1.0:1:3.4	dark brown-red	1.53
$C_{18}N(CH_3)(CH_2CH_2OH)_2Pt\_SnSe_4$	31.24, 5.67, 1.75	42.1	0.9:1:3.3	dark brown-red	1.53
$C_{20}N(CH_3)(CH_2CH_2OH)_2Pt\_SnSe_4$	33.23, 5.93, 1.64	41.5	1.1:1:3.5	dark brown-red	1.63
$C_{16}N(CH_3)(CH_2CH_2OH)_2Pt\_SnTe_4$	20.19, 3.62, 1.18	19.8	1.0:1:4.0	black	0.65
$C_{18}N(CH_3)(CH_2CH_2OH)_2Pt\_SnTe_4$	17.39, 3.21, 0.96	20.7	0.9:1:3.9	black	0.50
$C_{20}N(CH_3)(CH_2CH_2OH)_2Pt\_SnTe_4$	25.46, 4.70, 1.15	32.8	0.9:1:3.7	black	0.71

[a] Based on energy-dispersive spectroscopy (EDS) results. Semiquantitative microprobe analyses (EDS) were performed on a JEOL JSM-6400 scanning electron microscope (SEM) equipped with a Noran EDS system. Data acquisition was performed several times in different areas of pressed flat surfaces of powder samples using an accelerating voltage of 20 keV and 60-s accumulation time. The results were very close between each measurement, and quoted values were obtained from an average of four measurements.

influence the diameter of the micellar rods present, as framework assembly initiates, and affect the charge matching requirements between cations and anions. In response, the inorganic framework needs to adjust its composition from surfactant to surfactant to meet these requirements.

The overall analytical data show that there is no simple stoichiometric charge balancing formula to describe these compounds. This would be difficult, since at least three different inorganic species, namely $[SnQ_4]^{4-}$, $[Sn_2Q_6]^{4-}$, and Q^{2-}, exist in FM solution and all could serve as building blocks and incorporate simultaneously into the inorganic walls. This notion is supported by ^{119}Sn Mössbauer spectroscopy (see below) which shows multiple Sn sites in the structure. It is also supported by the observation that, after formation of the solids, the filtrate solutions were colorless and contained no residual $[Sn_xQ_y]^{4-}$ and Q^{2-} anions, suggesting that everything was incorporated in the solid.[20]

A schematic of the surfactant organization into micellar rods and the hexagonal order that results by close packing, along with $[Sn_2Q_6]^{4-}$ anions electrostatically attached to their surface, is shown in Figure 3. The inorganic framework develops in the space between the surfactant rods. This in between space involves two different regions: (a) the wall region sandwiched between two adjacent micellar rods (a double point) and possessing a 2-fold symmetry axis (defined here as 2-WR) and (b) the wall region found between three such rods (a triple point) with a 3-fold axis (defined as 3-WR). These regions are indicated in Figure 3. It is reasonable to expect the local structure and distribution of $Pt/[SnQ_4]^{4-}/[Sn_2Q_6]^{4-}/Q^{2-}$ species in 2-WR and 3-WR regions to be different.

The wall thickness at 2-WR can be assumed to be approximately constant across surfactants, since this double point is the closest to micellar cylinders can come to each other. This however is not the case at the triple point 3-WR whose proportion can be expected to grow as the micellar cylinder radius (i.e., surfactant chain length) increases. Thus we can conclude that, as the micellar rod diameter changes, the relative ratio of $Pt/[SnQ_4]^{4-}/[Sn_2Q_6]^{4-}/Q^{2-}$ species in the 2-WR/3-WR regions must also change. Therefore, the various members generated by changing the surfactant chain length have slightly different framework composition and are not formal chemical analogues where the framework stays chemically identical and the cationic surfactant simply changes.

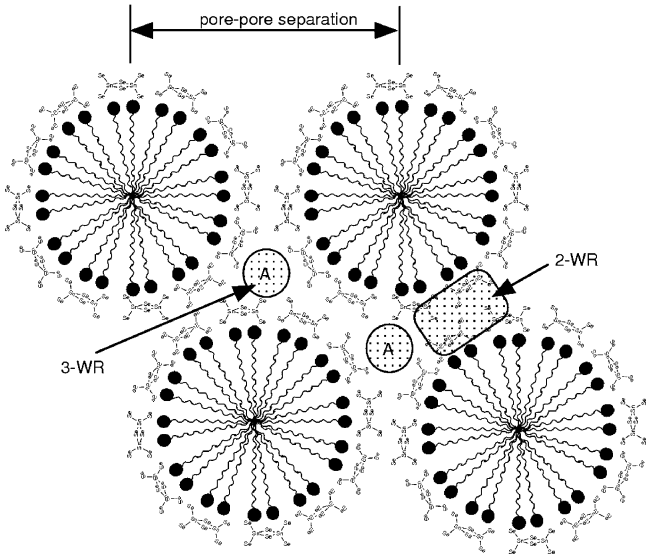

Figure 3. Schematic representation of electrostatic assembly of micellar surfactant rods and inorganic $[Sn_2Se_6]^{4-}$ anions that forms a hexagonal pore structure. The wall regions possessing a 3-fold axis and 2-fold axis denoted as 3-WR (A) and 2-WR (B).

Consistent with the above proposition are the results from ^{119}Sn Mössbauer spectroscopy (see Supporting Information). Each spectrum obtained from representative mesostructured selenides contains multiple components that correspond to different Sn environments with isomer shifts characteristic of Sn^{4+}. These environments could represent several types of $[Sn_xQ_y]^{n-}$ anions as well as several binding modes of a particular anion in the framework. Moreover, the number of components and the shape of each spectrum vary as a function of surfactant chain length and headgroup size and suggest that the relative distributions of the different anions vary.

(20) No precipitation of PbQ occurred when an aqueous solution of $Pb(NO_3)_2$ was added to the filtrate solution.

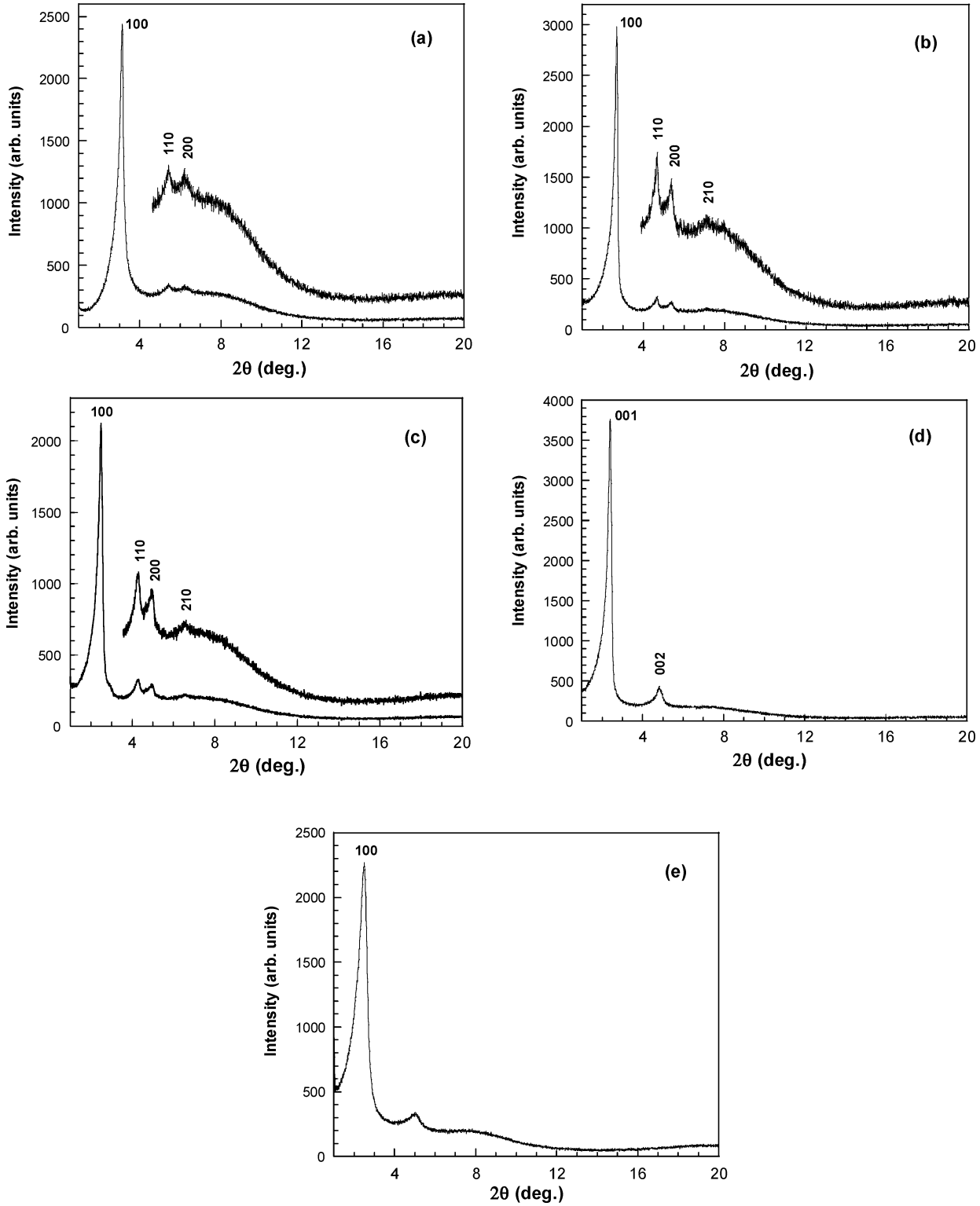

Figure 4. X-ray powder diffraction patterns of $C_nPyPt\_SnSe_4$ (a) $n = 12$, (b) $n = 14$, (c) $n = 16$, (d) $n = 18$, and (e) $C_{16}PyPd\_SnSe_4$ (Cu Kα rad).

Pore Order, Linkage Metal Ions, and Surfactant Chain Length. Shown in Figure 4 are the X-ray powder diffraction patterns of $C_nPyPt\_SnSe_4$ ($n = 12$, 14, 16, and 18) materials. For $n = 12$, 14, and 16, the patterns show three or four well-defined Bragg reflections in the $2° < 2\theta < 7°$ region, characteristic of regular hexagonal pore arrangement similar to those of well ordered silica MCM-41. This is in contrast to the system $(C_{16}Py)_{4-2x}M_xSnSe_4$ ($M = Mn^{2+}$, Fe^{2+}, Co^{2+}, Zn^{2+}, Cd^{2+}, Hg^{2+}),[5f] where, under identical experimental conditions, more disordered phases resulted. The divalent ions have a tetrahedral coordination preference and react nearly instantaneously upon contact with the selenostannate anions in solution. Moreover when the linkage metal ion is Pd^{2+}, which has a square planar coordination preference but it too reacts nearly instantaneously, the resulting mesophase was disordered as well; see Figure 4e. Notably, a similar difference in overall structural order between Pt^{2+} (reacts slower and gives ordered phases) and Pd^{2+} (reacts fast and gives disorder phases, both with the

Table 2. Observed Bragg Reflections with Diffraction Pattern Indexing for Mesostructured Platinum Tin Chalcogenides

mesophase	d_{100}, Å	d_{110}, Å	d_{200}, Å	d_{210}, Å	hexagonal unit cell constant, Å
C_{12}PyPt_$SnSe_4$	28.0	16.2	14.1		32.5
C_{14}PyPt_$SnSe_4$	32.6	18.8	16.4	12.4	37.9
C_{16}PyPt_$SnSe_4$	35.8	20.6	17.8	13.5	41.2
C_{18}PyPt_$SnSe_4$	36.6		18.4		lamellar
$C_{16}N(CH_3)_3$Pt_$SnSe_4$	33.0	19.1	16.5		32.8
$C_{18}N(CH_3)_3$Pt_$SnSe_4$	36.6	21.6	19.0		37.9
$C_{20}N(CH_3)_3$Pt_$SnSe_4$	41.9	24.3	21.1	15.9	42.3
$C_{16}N(CH_2CH_3)_3$Pt_$SnSe_4$	35.7				
$C_{18}N(CH_2CH_3)_3$Pt_$SnSe_4$	37.6	21.9	19.2		38.4
$C_{20}N(CH_2CH_3)_3$Pt_$SnSe_4$	40.7	23.9	20.7	15.7	41.4
$C_{16}N(CH_3)(CH_2CH_2OH)_2$Pt_$SnSe_4$	36.6	21.6	18.7	14.2	37.4
$C_{18}N(CH_3)(CH_2CH_2OH)_2$Pt_$SnSe_4$	38.1	22.1	19.3	14.7	38.7
$C_{20}N(CH_3)(CH_2CH_2OH)_2$Pt_$SnSe_4$	40.7	23.9	20.7	15.7	41.4
$C_{16}N(CH_3)(CH_2CH_2OH)_2$Pt_$SnTe_4$	34.9				
$C_{18}N(CH_3)(CH_2CH_2OH)_2$Pt_$SnTe_4$	36.6				
$C_{20}N(CH_3)(CH_2CH_2OH)_2$Pt_$SnTe_4$	38.6				

same coordination preference) was observed in mesostructured chalcogenides based on adamantane $[Ge_4Q_{10}]^{4-}$ (Q = S, Se) units.[21] Therefore, it would appear that the rate of reaction and framework assembly and not the coordination preference of the linkage metal are the predominantly controlling factors in allowing order to develop.

In the system C_nPyBr/K_2PtCl_4/K_4SnSe_4/FM, for $n = 18$ the decrease in surface curvature evidently allows the polar headgroups to pack more tightly favoring lamellar packing (see Figure 4d), while for $n < 18$ the packing favors hexagonal arrangement. Interestingly, this behavior was not observed with the more bulky $[Sn_4Se_{10}]^{4-}$ anion which afforded materials with hexagonal pore order up to $n = 22$.[9c] In that case the larger $[Sn_4Se_{10}]^{4-}$ anion enforces a higher surface curvature that favors hexagonal packing even when $n = 22$. It is perhaps no coincidence that in the system C_nPyBr/K_2PtCl_4/$K_4Sn_2Se_6$/FM ($n = 18$, 20) the intermediate size anion[22] $[Sn_2Se_6]^{4-}$ afforded (for the same surfactant) materials with cubic $Ia\bar{3}d$ symmetry.[11] It is noteworthy that, for the same surfactant, chain length, and linkage metal, i.e., C_{18}PyBr and Pt^{2+}, the sequence $[Sn_4Se_{10}]^{4-} > [Sn_2Se_6]^{4-} > [SnSe_4]^{4-}$ should result in decreasing micellar surface curvature and consequently in materials with *hexagonal P6mm, cubic* $Ia\bar{3}d$, and *lamellar* structure, respectively.

Varying the Surfactant Headgroup. In the system C_nPyBr/K_2PtCl_4/K_4SnSe_4/FM clearly the surfactant chain length plays a crucial role in controlling the long-range periodicity and overall framework structure in the solid (hexagonal or lamellar). To complete the investigation it is also important to look at the structure directing role of the headgroup. To do so we selected the surfactants depicted in Scheme 1. The headgroups in these vary in both size and shape.

The XRD patterns of $C_nN(CH_3)_3$Pt_$SnSe_4$ ($n = 16$, 18, 20) show Bragg reflections characteristic of regular hexagonal pore arrangement for n up to 20. That is in contrast with the pyridinium-based solids where the hexagonal pore order is observed for lengths of only up to $n = 16$. The long-range order of the pore structure, as judged by the relative intensities of the (110) and (200) reflections,[23] is not materially affected by the surfactant chain length. The pore−pore separation monotonically increases with chain length from 32.8 to 42.3 Å; see Table 2.

Scheme 1. Surfactants Employed for the Construction of Mesostructured Platinum Tin Chalcogenides (a) Alkyl-pyridinium, (b) Alkyl-trimethylammonium, (c) Alkyl-triethylammonium, and (d) Alkyl-methyl-diethanolammonium in the Form of Their Bromide Salts

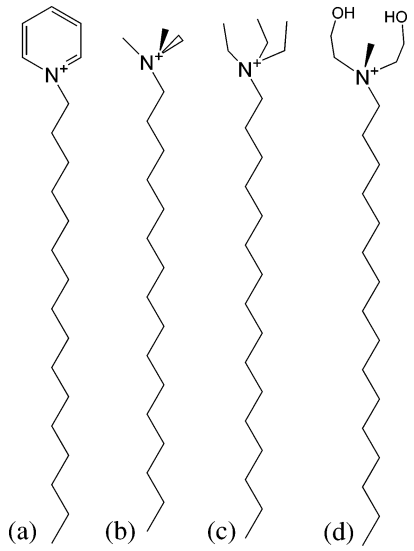

Surfactants with even larger headgroups such as alkytriethylammonium ($C_{20}N^+(CH_2CH_3)_3$) give material with excellent hexagonal symmetry. When $n = 18$ the long-range hexagonal pore order is markedly reduced as judged by the significant less intense (110) and (200) reflections, while for $n = 16$ these reflections are hardly present suggesting even less structural pore coherence in this solid. For the same chain length, the larger triethylammonium headgroup, compared to trimethylammonium and pyridinium, effectively increases the micelle rod surface curvature achieving good hexagonal pore order only for $n = 20$ and not for $n = 16$, 18.

The hydroxyl-functionalized surfactants $C_nN(CH_3)(CH_2CH_2OH)_2$Br ($n = 16$, 18, and 20) gave materials with the best hexagonal pore structure exhibiting the sharpest most intense X-ray diffraction patterns in the entire family, Figure 5. The pore−pore separation increases almost linearly with surfactant chain length in the range 37.4−41.4 Å (see Table 2), consistent with constant inorganic wall thickness.

(21) Trikalitis, P. N.; Rangan, K. K.; Kanatzidis, M. G. *Mater. Res. Soc. Symp. Proc.* **2002**, *703*, 433−438.
(22) The volume of $[Sn_2Se_6]^{4-}$ lies between that of $[Sn_4Se_{10}]^{4-}$ and $[SnSe_4]^{4-}$.
(23) Edler, K. J.; White, J. W. *Chem. Mater.* **1997**, *9*, 1226.

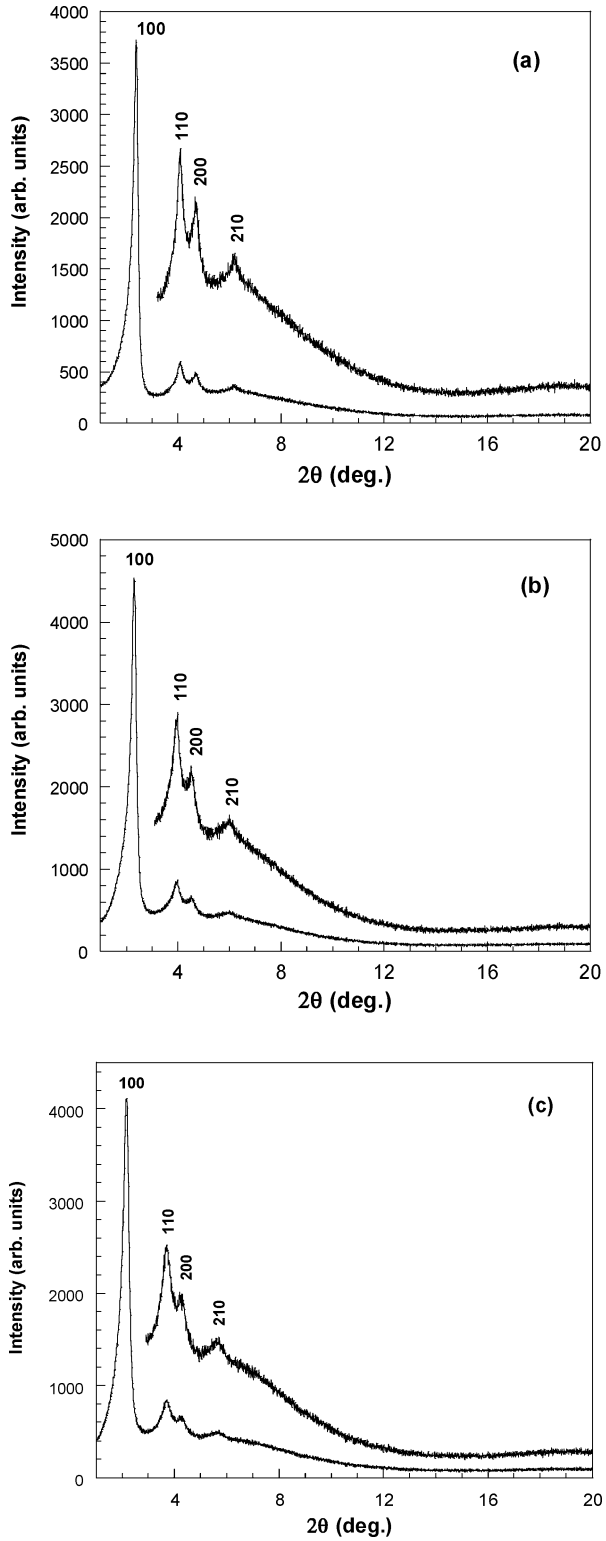

Figure 5. X-ray powder diffraction patterns of $C_nN(CH_3)(CH_2CH_2OH)_2Pt\_SnSe_4$ (a) $n = 16$, (b) $n = 18$, and (c) $n = 20$. All samples show four intense low angle Bragg reflections, characteristic of high quality hexagonal mesostructured material.

The pore organization and long-range order in mesostructured platinum tin selenide materials was investigated directly with TEM. Figures 6a and b show characteristic TEM images of $C_{16}PyPt\_SnSe_4$ and $C_{20}N(CH_3)(CH_2CH_2OH)_2Pt\_SnSe_4$ down the pore tunnel axis ([100] direction) where the hexagonal structure is clearly visible, coherent and extends throughout the particle.

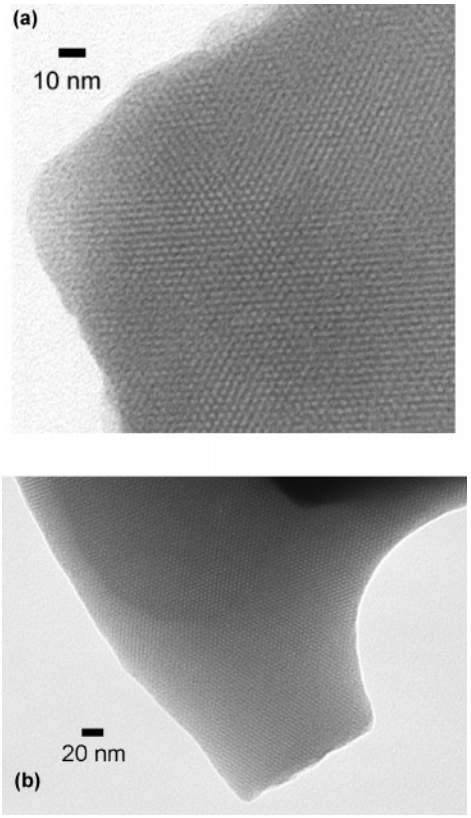

Figure 6. Representative TEM images of (a) $C_{16}PyPt\_SnSe_4$ and (b) $C_{20}N(CH_3)(CH_2CH_2OH)_2Pt\_SnSe_4$ down the pore tunnel axis.

Mesostructured Platinum Tin Tellurides. The heavier telluride-based materials are very attractive because of potentially interesting electrical properties arising from their anticipated lower energy band gaps. Yet, telluride members of the mesostructured chalcogenide family have been little investigated. The main reason is that access to the precursor anions $[MTe_4]$,$^{4-}$ $[M_2Te_6]^{4-}$ and $[M_4Te_{10}]^{4-}$ (M = Ge, Sn) is more difficult compared to the sulfide and selenide analogues.

Our initial attempts to synthesize mesostructured materials using $[SnTe_4]^{4-}$ as the precursor and various linkage metals, e.g., Ni^{2+}, Co^{2+}, Zn^{2+}, Cd^{2+}, Hg^{2+}, in FM resulted in either highly disordered or completely amorphous phases. The use of Pt^{2+} with its slower reaction kinetics gave more promising results. However, whereas the $[SnSe_4]^{4-}/Pt^{2+}$ combination afforded materials with excellent long-range hexagonal mesoscopic order, similarly ordered mesostructured solids based on $[SnTe_4]^{4-}$ anions proved more difficult to obtain. The reason might be because the rate of $Pt^{2+}/[SnTe_4]^{4-}$ coupling is faster compared to the $Pt^{2+}/[SnSe_4]^{4-}$ system.

X-ray diffraction patterns of $C_nN(CH_3)(CH_2CH_2OH)_2Pt\_SnTe_4$ materials show a strong, relatively sharp peak at low scattering angles corresponding to (100) reflections; see Figure 7. The patterns show also a broad peak at $2\theta \approx 3-5°$, which can be attributed to overlapping higher order reflections (110) and (200) of a hexagonal lattice, which is also observable by transmission electron microscopy (TEM). Figure 8a shows a characteristic TEM image of $C_{16}N(CH_3)(CH_2CH_2OH)_2Pt\_SnTe_4$ down the pore tunnel axis ([100] direction) where the hexagonal structure is clearly visible. Figure 8b shows a view of $C_{16}N(CH_3)(CH_2CH_2OH)_2Pt\_SnTe_4$ perpendicular to the pore channel ([110] direction) where long straight parallel tunnels are apparent.

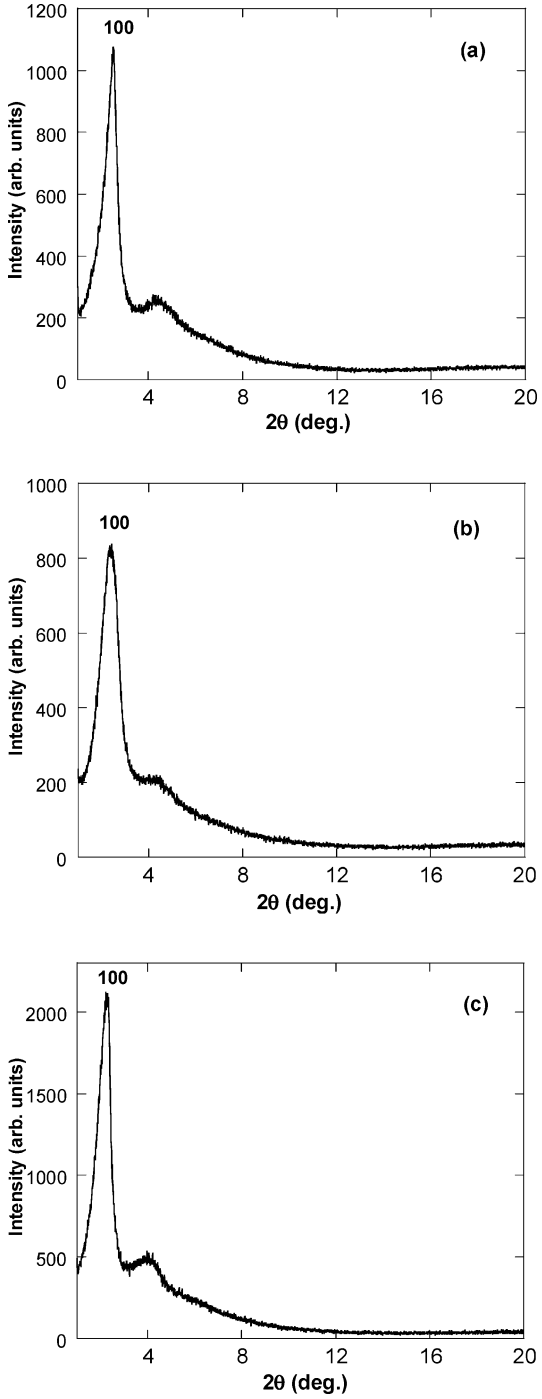

Figure 7. X-ray powder diffraction patterns of $C_nN(CH_3)(CH_2CH_2OH)_2Pt\_SnTe_4$ (a) $n = 16$, (b) $n = 18$, and (c) $n = 20$.

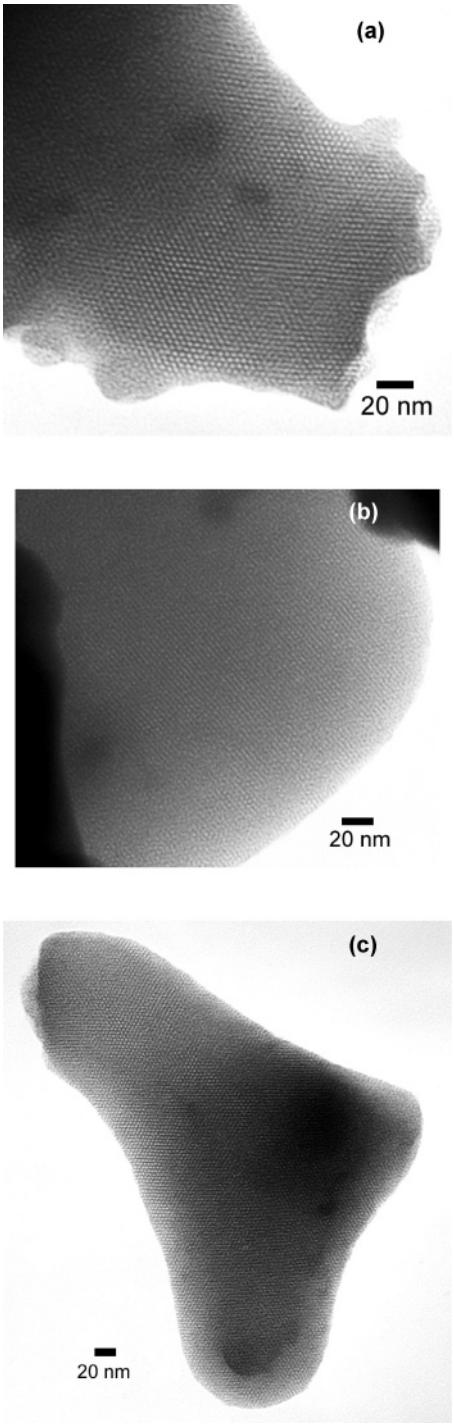

Figure 8. Representative TEM images of (a) $C_{16}N(CH_3)(CH_2CH_2OH)_2Pt\_SnTe_4$ down the pore tunnel axis, (b) $C_{16}N(CH_3)(CH_2CH_2OH)_2Pt\_SnTe_4$ perpendicular to the pore tunnel axis, and (c) large particle of $C_{16}N(CH_3)(CH_2CH_2OH)_2Pt\_SnTe_4$ showing the hexagonal organization extending over its full body.

Notably, in the same system some particles show the hexagonal organization to extend over their full body; see Figure 8c. In all cases the observed interpore distances are in good agreement with those obtained from the X-ray diffraction patterns (Table 2). The use of other surfactant templates such as alkylpyridinium and alkytrimethylammonium ions did not improve the pore order. In marked contrast with the selenide analogues, the corresponding tellurides were found to be significantly air sensitive.

Stability of Mesostructured Solids. The mesostructured platinum tin selenides are notably stable over time at room temperature. Samples exposed to air for several days showed XRD patterns that were identical to those of freshly prepared samples. On the contrary, the tellurides were found to be very air sensitive, and in many cases we even observed pyrophoric behavior. However under inert conditions the samples are stable for months.

The thermal stability was investigated with TGA and pyrolysis mass spectrometry (MS). Shown in Figure 9 are typical TGA curves of $C_{18}N(CH_3)(CH_2CH_2OH)_2Pt\_SnSe_4$, $C_{20}N(CH_3)_3Pt\_SnSe_4$, $C_{16}PyPt\_SnSe_4$, and $C_{20}N(CH_3)(CH_2CH_2OH)_2Pt\_SnTe_4$

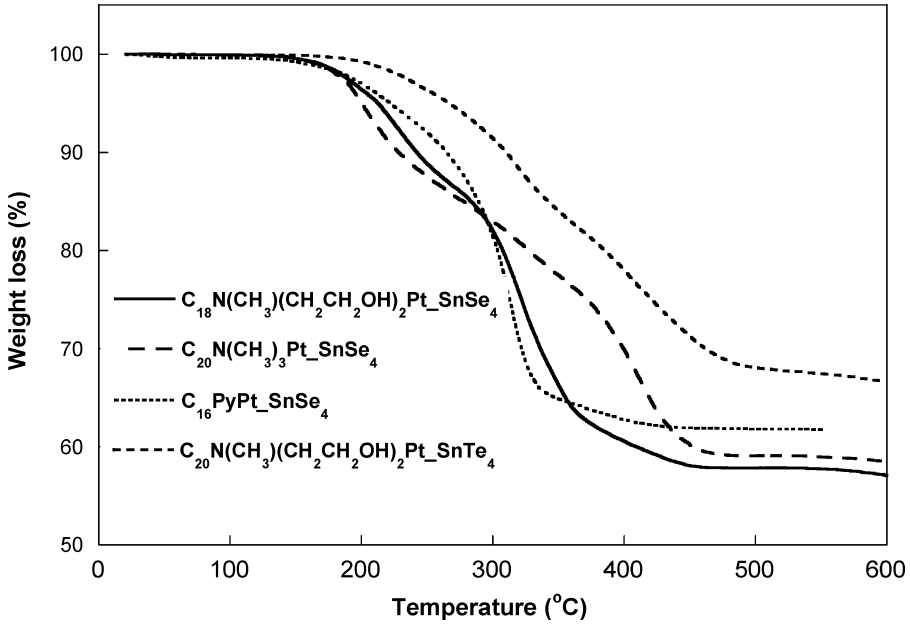

Figure 9. TGA curves of $C_{18}N(CH_3)(CH_2CH_2OH)_2Pt\_SnSe_4$, $C_{20}N(CH_3)_3Pt\_SnSe_4$, $C_{16}PyPt\_SnSe_4$, and $C_{20}N(CH_3)(CH_2CH_2OH)_2Pt\_SnTe_4$ under nitrogen flow (heating rate 10 deg/min).

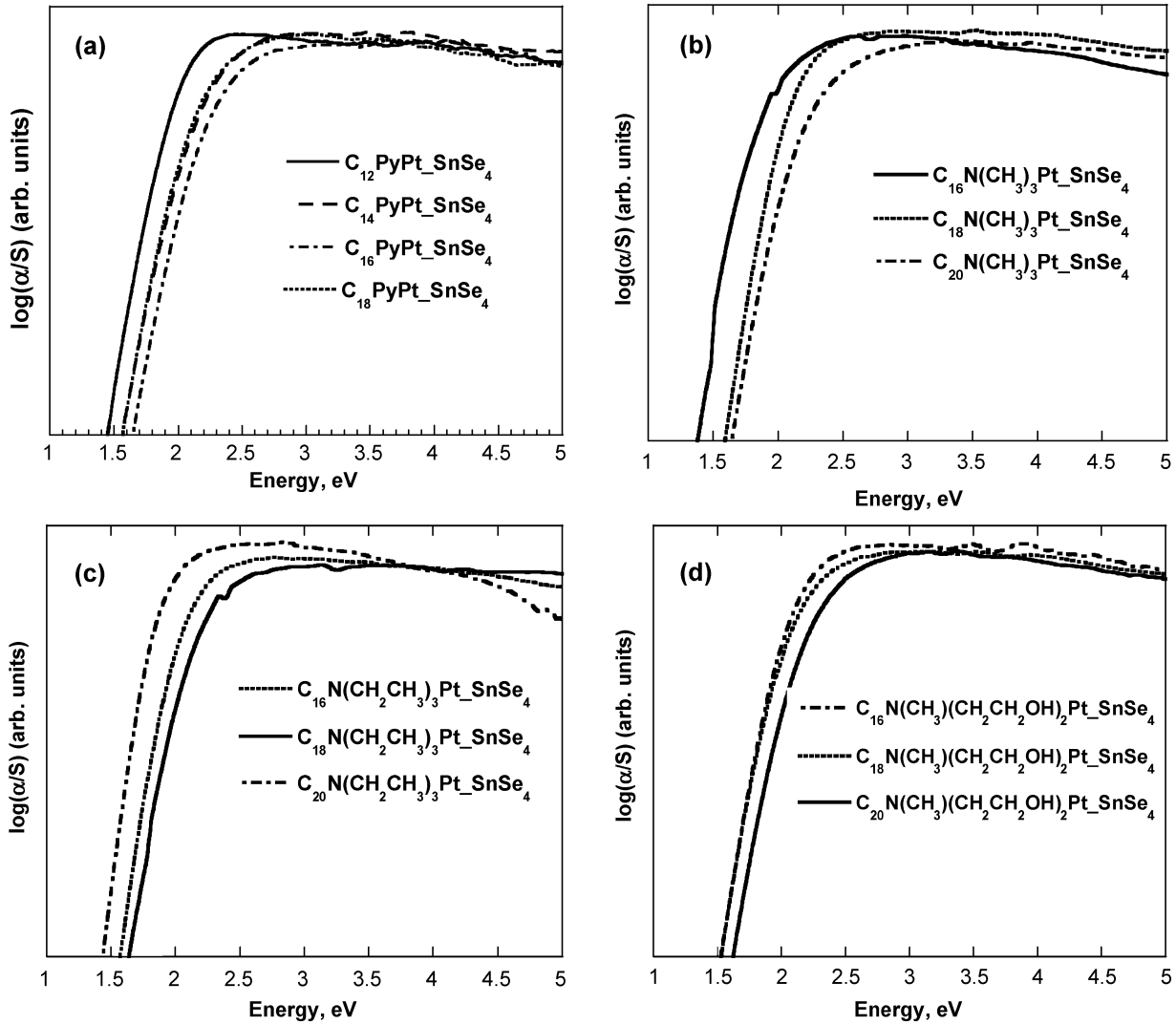

Figure 10. Solid-state UV−vis absorption spectra of (a) $C_nPyPt\_SnSe_4$, (b) $C_nN(CH_3)_3Pt\_SnSe_4$, (c) $C_nN(CH_2CH_3)_3Pt\_SnSe_4$, and (d) $C_nN(CH_3)(CH_2CH_2OH)_2Pt\_SnSe_4$ materials.

materials. The surfactant decomposition occurs between 150 and 500 °C via at least a two-step process as indicated from the slope change in the TGA curves. At ~600 °C the inorganic residue is a mixture of an amorphous and partially crystalline PtSnQ phase.

In the case of $C_nPyPt\_SnSe_4$, pyrolysis-MS experiments showed the major decomposition products to be the pyridyl headgroup and $C_nH_{2n+1}Se^+$. This pattern has been observed in all pyridinium-based mesostructured chalcogenides reported so far[9] suggesting a common mechanism of surfactant decomposition during which the inorganic framework is attacked. By contrast, no $R-Se^+$ was observed in the spectra of $C_nN(CH_3)(CH_2CH_2OH)_2Pt\_SnQ_4$, $C_nN(CH_2CH_3)_3Pt\_SnSe_4$, and $C_nN(CH_3)_3Pt\_SnSe_4$. The major species detected were the headgroups $N(CH_3)(CH_2CH_3)_2$ and $N(CH_3)_3$ along with $C_nH_{2n+1}N(CH_2CH_3)_2$, $C_nH_{2n+1}N(CH_3)(CH_2CH_3)$, and $C_nH_{2n+1}N(CH_3)_2$.

Optical Properties. The mesoporous materials described here, with the large, continuous periodic pores running through the Pt/Sn/Se frameworks, can be regarded as hybrid organic/inorganic systems. The absence of any residual chloride or bromide in these materials suggests that the metathesis of all ligands in $[PtCl_4]^{2-}$ was complete and the linking/polymerization reaction has produced a continuous, extended Pt/Sn/Se anionic framework[24] of covalently bonded atoms that encapsulates the surfactant molecules in its hexagonally packed pores. These frameworks are expected to have semiconducting properties in much the same fashion as regular dense crystalline or amorphous semiconductors do. This means a well-defined energy gap with a valence band composed of filled states of predominantly Se orbitals and a conduction band composed of empty states made primarily of Pt and Sn orbitals.

The energy gap is in fact fully developed and readily observable in these systems. The spectra in Figure 10 show sharp optical absorptions associated with band gap transitions in the energy range 1.4−1.7 eV (see Table 1). Interestingly, for materials with hexagonal pore symmetry and for the same kind of surfactant (e.g., alkylpyridinium), the absorption edge which defines the energy gap of the materials depends on the chain length. In all cases the energy band gap narrows in going from the longer to the shorter chain with an exception for $C_{20}N(CH_2CH_3)Pt\_SnSe_4$. This trend among the various types of organic templates may be understood in terms of variations in the chemical composition of the inorganic framework as a function of a surfactant chain length. In other words the inorganic framework seems to adjust slightly its composition to respond to the changing micellar rod diameter, according to the demands imposed by the double point (2-WR) and triple point (3-WR) regions (Figure 3) discussed above.

The optical absorption spectra of $C_nN(CH_3)(CH_2CH_2OH)_2Pt\_SnTe_4$ (see Supporting Information) show band gap transitions in the range 0.5−0.7 eV and are the lowest among the mesostructured chalcogenide solids observed so far.[9]

Concluding Remarks

One of the main new ideas derived from this work is that the construction of well ordered periodic mesostructured chalcogenide framework materials probably is favored if multiple anionic building units are present. These may form in situ from the precursor molecules used. In FM solution the $[SnQ_4]^{4-}$ anions serve as precursors and undergo conversion equilibria that generate additional species such as $[Sn_2Q_6]^{4-}$ and Q^{2-} and proceed to give materials with ordered pores. In water the $[SnQ_4]^{4-}$ anions remain intact and the products have disordered wormhole structures. This is a profound difference in behavior and has salient consequences in the long-range order and structure of the final mesostructures formed with Pt^{2+} ions and presumably many other metal ions. The results imply that M^{n+} and $[SnSe_4]^{4-}$ alone may not be sufficient to build an inorganic wall framework that can support a periodic pore structure. To build ordered mesostructures the system seems to require more than two anionic building blocks to properly construct the 2-WR as well the 3-WR regions defined in Figure 3. The species generated by the equilibria represent a collection of building blocks that could be used to supply the periodic structure with all the necessary "pieces". This conclusion may appear somewhat counterintuitive to expectations that call for ordered structures to result from simple well-defined starting materials and for disordered, untidy structures to result from mixtures of species of varying and unknown distribution. Additional experimental work involving these and other precursor systems is, however, required to further validate this multiple building block hypothesis.

The present work also illustrates the key role of Pt^{2+} as the linkage metal ion for the construction of hexagonal mesostructured chalcogenides from soluble K_4SnQ_4 (Q = Se, Te) salts in the presence of surfactant templates. At this point it is important to note the absence of cubic phases in the entire series of the surfactant/K_2PtCl_4/K_4SnSe_4/FM system. Given that the $C_nPy/K_2PtCl_4/K_4Sn_2Se_6$/FM ($n$ = 18, 20) system afforded materials with cubic crystal symmetry, the results reported here clearly underscore the importance of chalcogenide precursors in achieving a given pore symmetry. We can now discern a relationship between the formation of hexagonal *p*6*mm*, cubic $Ia\bar{3}d$, and lamellar phases and the respective size of building block (e.g., $[SnSe_4]^{4-}$, $[Sn_2Se_6]^{4-}$, and $[Sn_4Se_{10}]^{4-}$). A similar relationship has been observed in organic liquid crystals and mesoporous silicates and can be understood in terms of surface curvature and packing parameter of the organic/inorganic ion pair.[25]

Acknowledgment. This research was supported by NSF Grant CHE-0211029 (Chemistry Research Group). This work made use of the SEM and TEM facilities of the Center for Advanced Microscopy at MSU.

Supporting Information Available: Mössbauer spectra, table of isomer shifts and quadrupole splittings, optical absorption spectra. This material is available free of charge via the Internet at http://pubs.acs.org.

JA0447614

(24) The absence of any chloride atoms in the materials suggests a complete metathesis of the ligands of $[PtCl_4]^{2-}$ by the Se atoms.

(25) Huo, Q. S.; Margolese, D. I.; Stucky, G. D. *Chem. Mater.* **1996**, *8*, 1147−1160.